Copper Corrosion Protection by 4-Hydrocoumarin Derivatives: Insight from Density Functional Theory, Ab Initio, and Monte Carlo Simulation Studies

Saprizal Hadisaputra[1*], Agus Abhi Purwoko[1], and Saprini Hamdiani[2]

[1]*Chemistry Education Division, Faculty of Teacher Training and Education, University of Mataram, Jl. Majapahit No. 62, Mataram, 83125, Indonesia*

[2]*Department of Applied Chemistry, Chaoyang University of Technology, No. 168, Jifeng E. Rd., Wufeng District, Taichung 41349, Taiwan*

* ***Corresponding author:***

email: rizal@unram.ac.id

Received: October 3, 2021
Accepted: January 17, 2022

DOI: 10.22146/ijc.69530

Abstract: *The corrosion inhibition performance of 4-hydrocoumarin derivatives has been studied using weight loss, electrochemical impedance spectroscopy, potentiodynamic polarization, and electrochemical frequency modulation techniques. However, experimental studies have not explained why the methoxy (OCH_3) group contributes more to the increase in corrosion inhibition than the methyl (CH_3) and chlorine (Cl) functional groups. In this theoretical study, the electronic aspect of the target corrosion inhibitors will be studied in detail to help strengthen the explanation in the experimental research. Density functional theory,* ab initio*, and Monte Carlo simulations have been used to analyze the corrosion inhibition performance of 4 curcumin derivatives against copper. The quantum chemistry approach is carried out under gas and aqueous conditions in neutral and protonated inhibitors. The Monte Carlo simulation was used to observe the dynamics and the mechanism of inhibition of the target molecule on the copper surface. The quantum chemistry approach can mimic the geometrical parameters of molecular inhibitors. It can also explain electronically why the OCH_3 functional group is superior to other substituents. The adsorption energy of the 4-hydroquinone derivative is linearly correlated with the reported experimental study. The level of corrosion inhibition efficiency is $OCH_3 > CH_3 > H > Cl$.*

Keywords: *copper; corrosion inhibitor; DFT;* ab initio *MP2; Monte Carlo; 4-hydrocoumarin*

■ INTRODUCTION

Efforts to find green corrosion inhibitors that are economical, effective, but environmentally friendly are still intensive. Reports show that organic inhibitors are efficient for preventing the corrosion of metals [1-6]. Organic inhibitors have phi bonds and N, O, S heteroatom groups with high electron density, acting as active sites to interact with metal surfaces [7-10]. Organic inhibitors will donate electrons to the empty d orbital of the metal so that complex compounds will be formed. The adsorption of organic molecules on the metal surface can limit the initial contact of the metal with the corrosive environment so that the corrosion process can be prevented [11-12].

Experimental studies on the performance of organic inhibitors have been widely published, especially in preventing the corrosion of copper [13-16]. Jmiai et al. [17] tested the corrosion inhibitor of Jujube shell extract on copper in hydrochloric acid media. The corrosion inhibition efficiency value of Jujube shell extract against copper was 91%. Fouda et al. [18] tested four hydrocoumarin derivatives as corrosion inhibitors, namely 4-hydroxy-3-phenylazobenzopyrane-2-one (4HD-OCH_3), 4-hydroxy-3-(*p*-methylphenylazo)-benzopyrane-2-one (4HD-CH_3), 4-hydroxy-3-(*p*-methoxyphenyl azo)-benzopyrane-2-one (4HD-CH), and 4-hydroxy-3-(*p*-chlorophenylazo)-benzopyrane-2-one (4HD-Cl), on copper in nitric acid medium. The

highest corrosion inhibition efficiency value was given by 4HD-OCH_3, with a value of 94.9%. However, the report of Fouda et al. has not explained in more detail why 4HD-OCH_3 has the highest inhibition efficiency compared to other derivatives. Therefore, the current study focuses on bridging these problems theoretically. This study explains why the OCH_3 functional group contributes maximally to corrosion inhibition efficiency compared to CH_3 and Cl. Theoretical studies have reported many corrosion inhibition performances of various compounds [19-23]. Methods such as DFT and *ab initio* [24-30] can explain the electron distribution when the inhibitor interacts with the metal surface. The Monte Carlo simulation can define the orientation of each inhibitor molecule when interacting with the metal surface and show the adsorption pattern that occurs [31-32].

■ COMPUTATIONAL METHODS

Quantum Chemical Calculations

Quantum chemical calculations were carried out to predict the molecular structure, electron distribution, and electron transfer from corrosion inhibitors (4HC–H, 4HC–CH_3, 4HC–OCH_3, and 4HC–Cl) to the copper metal surface. The structure of targeted inhibitor molecules can be seen in Fig. 1. Geometry optimization is carried out first using the DFT method B3LYP/6-31G(d) to speed up the calculation of molecular geometry. The structures of 4HC–H, 4HC–CH_3, 4HC–OCH_3, and 4HC–Cl were re-optimized using the DFT and *ab initio* MP2 methods at the theoretical level 6-311++G (d,p) in the gas phase, for both neutral and protonated molecules. A polarized continuum model based on the Gaussian code is used to incorporate the effect of solvent in the calculation. Water has a dielectric constant of 78.4, and other solvents follow the gaussian code. The gas-phase geometries from single-point estimates are sufficient for energetics in the solvent phase. Previous studies showed that it had only a small effect on structure and energy [33-35]. All calculations of quantum chemical and geometric parameters using the Gaussian 09 program [36].

Quantum chemical parameters such as high occupied and low unoccupied molecular orbitals (EHOMO and ELUMO), gap energy ΔE, ionization potential (I),

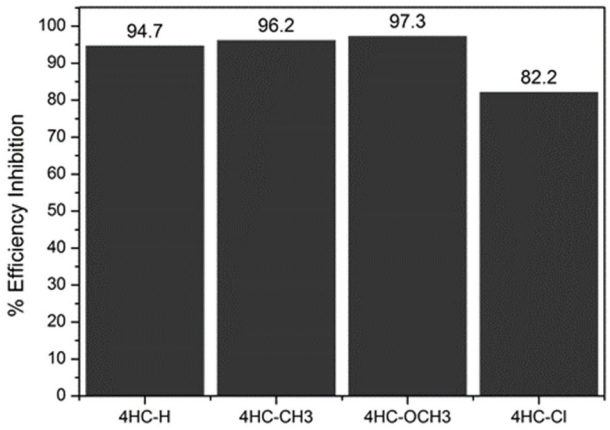

Fig 1. The efficiency of corrosion inhibition of 4-hydrocoumarin derivatives against copper [18]

electron affinity (A), electronegativity (χ), hardness (η), and the number of electron transfers (ΔN) were calculated based on DFT and *ab initio* methods. According to Koopman's theorem, the energy values of HOMO and LUMO in each organic inhibitor are related to the ionization potential (I) and electron affinity (A) [37] according to Eq. 1 and Eq. 2.

$$I = -EHOMO \quad (1)$$

$$A = -ELUMO \quad (2)$$

Electronegativity (χ) and hardness of each organic inhibitor can be calculated by Eqs. 3 4 [38-39]:

$$\chi = \frac{(I + A)}{2} \quad (3)$$

$$\eta = \frac{(I - A)}{2} \quad (4)$$

According to Pearson's theory [40-41], the number of electrons transferred (ΔN) from each organic inhibitor to the metal can be calculated by Eq. 5.

$$\Delta N = \frac{\chi Cu - \chi Inh}{2(\eta CU + \eta Inh)} \quad (5)$$

where χCu and χInh represent absolute electronegativity values of copper and organic inhibitors, respectively. ηCu and ηInh, respectively, represent absolute hardness values of copper and organic inhibitors. The theoretical study values of χCu = 4.48 eV/mol and ηCu = 0 eV/mol were used to calculate the number of electrons transferred [42].

The Fukui index to determine nucleophilic (f^+) and electrophilic (f^-) attacks [43] can be calculated by Eq. 6 and Eq. 7.

$$f^{+} = q_k(N+1) q_k(N) \quad (6)$$

$$f^{-} = q_k(N) - q_k(N-1) \quad (7)$$

where $q_k(N+1)$ is atomic charge (+1), $q_k(N)$ is atomic charge (0), $q_k(N-1)$ is atomic charge (-1) in organic inhibitors. f^{+} indicates that the attack is nucleophilic while f^{-} indicates that the attack is electrophilic [43].

Monte Carlo Simulation

The interactions between organic inhibitors, water molecules, and metal surfaces were studied using the Material Studio software [44-45]. The Monte Carlo simulation can help find the most stable adsorption site on the metal surface by searching for the lowest energy adsorption site. The Monte Carlo simulation protocol in this study uses the steps as previously published [46]. All simulations are implemented with the COMPASS force field to optimize all system components. The adsorbates used in this simulation are 4HC–H, 4HC–CH_3, 4HC–OCH_3, and 4HC–Cl. Each adsorbate added 100 molecules of water to simulate the effect of the solvent because corrosion occurs in the solution. The simulation aims to find the lowest energy adsorption side to determine the adsorption preference of organic inhibitors on the surface of Cu(111) in 100 water molecules.

■ RESULTS AND DISCUSSION

Experimental studies on 4-Hydrocoumarin derivatives as corrosion inhibitors on copper in nitric acidmedia have been reported by Fouda et al. [18]. The highest inhibition efficiency value in 4H–OCH_3 was obtained at 97.3%, according to Fig. 1. From the experimental study, it was seen that the OCH_3 group gave the maximum contribution to the efficiency of corrosion inhibition. However, in the publication, Fouda et al. [18] have not explained why OCH_3 contributes more to the corrosion inhibition performance than the CH_3 and Cl functional groups. Revisiting the corrosion inhibition performance of 4-hyrdrocoumarin derivatives was remodeled using DFT, *ab initio*, and Monte Carlo simulation studies. The structures of derivatives of 4-hyrocoumarin such as 4HC–H, 4HC–CH_3, 4HC–OCH_3, and 4HC–Cl are depicted in Fig. 2. The four corrosion inhibitors were tested theoretically as corrosion inhibitors on copper surfaces.

First, the DFT and *ab initio* methods determine the geometry and quantum chemical parameters. As a consequence of choosing the DFT and *ab initio* methods, it is necessary to validate its accuracy. The theoretical level validation was carried out by comparing the crystal structure of the 4-hydrocoumarin derivative with the theoretical results [47]. A comparison of experimental and theoretical geometry parameters can be seen in Table 1. There is a relatively low difference between bond distance and bond angle between DFT/6-311++G (d,p) and experimental, 0.016 and 0.818, respectively. It shows that the level theory for testing corrosion inhibition is accurate.

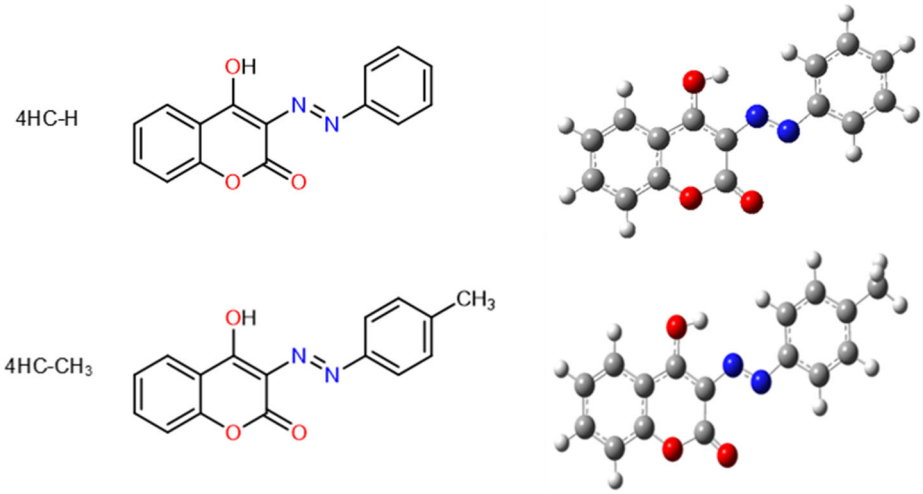

Fig 2. 2D and 3D structures of the inhibitors, 4HC-H, 4HC-CH_3, 4HC-OCH_3, and 4HC-Cl

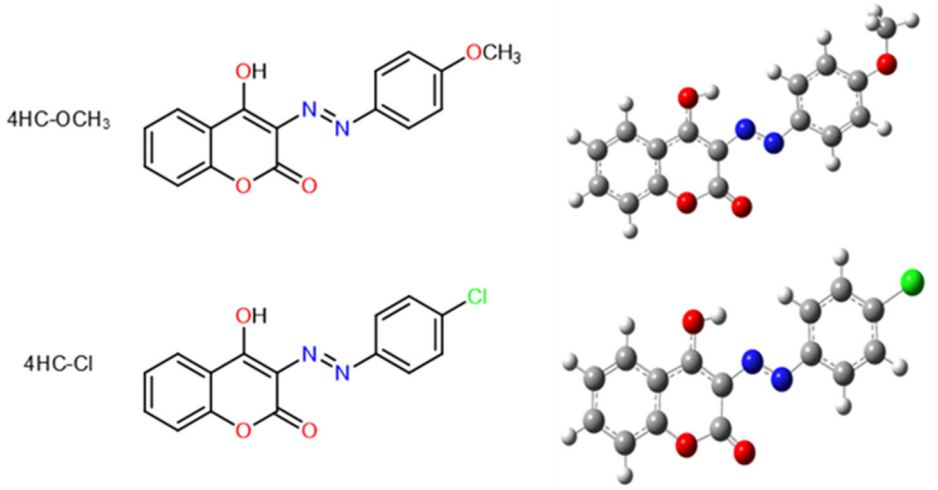

Fig 2. 2D and 3D structures of the inhibitors, 4HC-H, 4HC-CH_3, 4HC-OCH_3, and 4HC-Cl (*Continued*)

Table 1. Comparison of geometrical parameters from X-ray structure of the 4-hydrocoumarin [32] and DFT/6-311++G (d,p)

Bond (Å)	Exp. [32]	Theory	Angle (°)	Exp. [32]	Theory
C(1)-O(1)	1.199	1.202	O(2)-C(2)-C(3)	116.7	117.443
C(1)-O(2)	1.378	1.414	O(2)-C(2)-C(7)	121.9	122.036
C(1)-C(9)	1.450	1.464	C(3)-C(2)-C(7)	121.4	120.520
O(2)-C(2)	1.371	1.358	C(2)-C(3)-C(4)	118.9	119.181
C(2)-C(3)	1.374	1.398	C(3)-C(4)-C(5)	120.6	120.952
C(2)-C(7)	1.384	1.407	C(6)-C(5)-C(4)	120.5	119.868
C(3)-C(4)	1.376	1.390	C(5)-C(6)-C(7)	119.3	120.022
C(4)-C(5)	1.387	1.405	C(2)-C(7)-C(6)	119.3	119.457
C(5)-C(6)	1.372	1.386	C(2)-C(7)-C(8)	117.3	116.739
C(6)-C(7)	1.398	1.409	C(6)-C(7)-C(8)	123.4	123.805
C(7)-C(8)	1.435	1.436	O(3)-C(8)-C(9)	123.3	120.411
C(8)-O(3)	1.310	1.334	O(3)-C(8)-C(7)	115.6	118.067
C(8)-C(9)	1.375	1.390	C(9)-C(8)-C(7)	121.1	121.522
-	-	-	C(8)-C(9)-C(1)	120.0	120.810

EHOMO is associated with the ability to donate electrons from molecules to metals. The EHOMO value indicates the tendency of the molecule to donate electrons to the acceptor molecule [37]. Therefore, the higher the EHOMO value, the stronger the organic inhibitor molecules attached to the metal surface. Prediction of organic inhibitors with the highest corrosion inhibition efficiency value can be based on the EHOMO value. Tables 2, 3, 4, and 5 show the quantum parameters of the 4-hydrocoumarin derivatives calculated using the DFT/6-311++G and MP2/6-311++G methods—calculation of quantum chemical parameters based on Eqs. 1, 2, 3, 4, and 5. Tables 2, 3, 4, and 5 show that the highest EHOMO values correlate with the order of corrosion inhibition efficiency values in copper. The order of EHOMO values is 4HC–OCH_3 > 4HC–CH_3 > 4HC–H> 4HC–Cl. It can be seen that 4HC–OCH_3 has a higher EHOMO compared to other inhibitors. Table 3, for example, shows that the EHOMO value of 4HC–OCH_3 is the largest, -8.0233 eV. The results of a linear theoretical study with experimental results that have been previously reported by Fouda et al. [18]. The distribution of electrons in the HOMO orbitals of the four inhibitors is visualized in Fig. 3.

Table 2. The quantum chemical parameters (in eV) of neutral 4-hydrocoumarin derivatives were calculated using B3LYP/6-311++G(d,p) and MP2/6-311++G(d,p) in the gas phase

	EHOMO	ELUMO	ΔE	*I*	*A*	χ	η	ΔN
4HC-H								
B3LYP/6-311++G(d,p)	-6.4458	-2.9603	-3.4855	6.4458	2.9603	4.7031	1.7428	-0.0640
MP2/6-311++G(d,p)	-8.2429	0.5761	-8.8189	8.2429	-0.5761	3.8334	4.4095	0.0733
4HC-CH_3								
B3LYP/6-311++G(d,p)	-6.2959	-2.8719	-3.4240	6.2959	2.8719	4.5839	1.7120	-0.0303
MP2/6-311++G(d,p)	-8.0644	0.6585	-8.7229	8.0644	-0.6585	3.7029	4.3614	0.0890
4HC-OCH_3								
B3LYP/6-311++G(d,p)	-6.0665	-2.7952	-3.2714	6.0665	2.7952	4.4308	1.6357	0.0150
MP2/6-311++G(d,p)	-7.8913	0.7064	-8.5977	7.8913	-0.7064	3.5924	4.2989	0.1032
4HC-Cl								
B3LYP/6-311++G(d,p)	-6.4997	-3.1007	-3.3990	6.4997	3.1007	4.8002	1.6995	-0.0942
MP2/6-311++G(d,p)	-8.3493	0.4079	-8.7572	8.3493	-0.4079	3.9707	4.3786	0.0581

Table 3. The quantum chemical parameters (in eV) of neutral the 4-hydrocoumarin derivative were calculated using B3LYP6-311++G(d,p) and MP2/6-311++G(d,p) in the aqueous phase

	EHOMO	ELUMO	ΔE	*I*	*A*	χ	η	ΔN
4HC-H								
B3LYP/6-311++G(d,p)	-6.5454	-3.0153	-3.5301	6.5454	3.0153	4.7804	1.7651	-0.0851
MP2/6-311++G(d,p)	-8.3558	0.5524	-8.9082	8.3558	-0.5524	3.9017	4.4541	0.0649
4HC-CH_3								
B3LYP/6-311++G(d,p)	-6.4050	-2.9560	-3.4490	6.4050	2.9560	4.6805	1.7245	-0.0581
MP2/6-311++G(d,p)	-8.1876	0.6052	-8.7928	8.1876	-0.6052	3.7912	4.3964	0.0783
4HC-OCH_3								
B3LYP/6-311++G(d,p)	-6.1707	-2.9013	-3.2694	6.1707	2.9013	4.5360	1.6347	-0.0171
MP2/6-311++G(d,p)	-8.0233	0.6425	-8.6657	8.0233	-0.6425	3.6904	4.3329	0.0911
4HC-Cl								
B3LYP/6-311++G(d,p)	-6.5321	-3.0801	-3.4520	6.5321	3.0801	4.8061	1.7260	-0.0945
MP2/6-311++G(d,p)	-8.3890	0.4740	-8.8630	8.3890	-0.4740	3.9575	4.4315	0.0590

Table 4. Quantum chemical parameters (in eV) of protonated 4-hydrocoumarin derivative calculated using B3LYP6-311++G(d,p) and MP2/6-311++G(d,p) in the gas phase

	EHOMO	ELUMO	ΔE	*I*	*A*	χ	η	ΔN
Pronated 4HC-H								
B3LYP/6-311++G(d,p)	-9.8622	-6.4328	-3.4295	9.8622	6.4328	8.1475	1.7147	-1.0694
MP2/6-311++G(d,p)	-11.5624	-2.8945	-8.6679	11.5624	2.8945	7.2284	4.3340	-0.3171
Pronated 4HC-CH_3								
B3LYP/6-311++G(d,p)	-9.5580	-6.3296	-3.2284	9.5580	6.3296	7.9438	1.6142	-1.0729
MP2/6-311++G(d,p)	-11.2348	-2.8169	-8.4178	11.2348	2.8169	7.0258	4.2089	-0.3024
Pronated 4HC-OCH_3								
B3LYP/6-311++G(d,p)	-9.1349	-6.2385	-2.8964	9.1349	6.2385	7.6867	1.4482	-1.1071
MP2/6-311++G(d,p)	-10.9499	-2.7807	-8.1691	10.9499	2.7807	6.8653	4.0846	-0.2920
Pronated 4HC-Cl								
B3LYP/6-311++G(d,p)	-9.9420	-6.7599	-3.1821	9.9420	6.7599	8.3509	1.5911	-1.2165
MP2/6-311++G(d,p)	-11.8078	-3.1984	-8.6094	11.8078	3.1984	7.5031	4.3047	-0.3511

Table 5. The derived quantum chemical parameters (in eV) of protonated 4-hydrocoumarin were calculated using B3LYP6-311++G(d,p) and MP2/6-311++G(d,p) in the aqueous phase

	EHOMO	ELUMO	ΔE	*I*	*A*	χ	η	ΔN
Pronated 4HC-H								
B3LYP/6-311++G(d,p)	-7.1128	-3.4349	-3.6779	7.1128	3.4349	5.2738	1.8389	-0.2158
MP2/6-311++G(d,p)	-8.8987	0.1981	-9.0968	8.8987	-0.1981	4.3503	4.5484	0.0143
Pronated 4HC-CH_3								
B3LYP/6-311++G(d,p)	-6.9084	-3.3737	-3.5348	6.9084	3.3737	5.1410	1.7674	-0.1870
MP2/6-311++G(d,p)	-8.6709	0.2397	-8.9106	8.6709	-0.2397	4.2156	4.4553	0.0297
Pronated 4HC--OCH_3								
B3LYP/6-311++G(d,p)	-6.5819	-3.3157	-3.2662	6.5819	3.3157	4.9488	1.6331	-0.1435
MP2/6-311++G(d,p)	-8.4614	0.2672	-8.7286	8.4614	-0.2672	4.0971	4.3643	0.0439
Pronated 4HC-Cl								
B3LYP/6-311++G(d,p)	-7.1253	-3.6616	-3.4637	7.1253	3.6616	5.3934	1.7319	-0.2637
MP2/6-311++G(d,p)	-9.0040	-0.0041	-8.9999	9.0040	0.0041	4.5040	4.4999	-0.0027

EHOMO is directly related to the value of the ionization potential [38]. The potential ionization value can be calculated by Eq. 1. Table 4 shows that the lowest ionization potential value is indicated by 4HC-OCH_3 (8.0233 eV) compared to the potential ionization value of 4HC-H (8.3558 eV), 4HC-CH_3 (8.1876 eV), and 4HC-Cl (8.3890 eV). Based on the potential ionization value, it can be predicted that 4HC-OCH_3 has a higher inhibition efficiency value than 4HC-H, 4HC-CH_3, and 4HC-Cl. The value of ionization potential is the minimum energy required for the release of electrons to bind to the metal surface to protect the metal from corrosive media. Therefore, a low ionization potential value can increase the inhibition efficiency [38].

Electronegativity (χ) has proven to significantly influence the theory of chemical reactivity. When organic inhibitors and copper metal interact, electrons will flow from a lower electronegativity value (organic inhibitor) to a high electronegativity value (Cu) so that the chemical potential is balanced [39]. Electronegativity values were calculated using Eq. 3. Table 3 shows the calculations using the MP2/6-311++G(d,p) method. The lowest electronegativity value at 4HC–OCH_3 was 3.6904 eV. The electronegativity values for the other molecules 4HC–H, 4HC–CH_3, and 4HC–Cl were 3.9017, 3.7912, and 3.9575 eV, respectively. Based on the electronegativity value, it can be predicted that 4HC–OCH_3 has the highest corrosion inhibition efficiency value compared to the other three inhibitors. The value of electronegativity was obtained in linear theoretical calculations with experimental studies from Fouda et al. [18].

The number of electrons transferred (ΔN) from the inhibitor to the metal is calculated using Eq. 5. The electron transfer value shows that the electron donor's inhibition efficiency value is generated [37]. If the electron transfer value is less than 3.6, then the value of the inhibition efficiency increases. Electron transfer can occur in inhibited corrosion processes [38]. Inhibitors 4HC–H, 4HC–CH_3, 4HC–OCH_3, and 4HC–Cl are electron donors, while copper metal is an acceptor to produce an inhibitory adsorption layer against corrosion. More inhibitors will coat the Cu surface with the increased ability to donate electrons to the Cu surface. The order of high to low electron transferability is 4HC–OCH_3 > 4HC–CH_3 > 4HC–H > 4HC–Cl. These results are valid for all gaseous media and solution phases and neutral and protonated conditions. This trend of electron donors could explain why the OCH_3 functional group contributes to corrosion inhibition efficiency.

Molecular Electrostatic Potential (MEP) explains hydrogen bonding, reactivity, and the structural relationship of molecular activity. The structure of the electron density surface plot mapped by MEP describes the shape, size, distribution of charge density, and the place of chemical reactivity in a molecule. The color

scheme for the MEP surface is red, indicating electron-rich and partially negative charge; blue color indicates a lack of electrons and a partial positive charge; a light blue color indicates a slightly electron-deficient region; the yellow color indicates a slightly electron-rich region; and green color indicates neutral [48]. The MEP plots of the targeted organic inhibitors 4HC–H, 4HC–CH_3, 4HC–OCH_3, and 4HC-Cl can be seen in Fig. 3. Low electron density in blue is seen in the delocalized region of benzene. The electron density is higher in the red to the green color of the oxygen atom in the carbonyl of the coumarin structure. It shows that the oxygen atom in the carbonyl of the coumarin structure has a high electron density. It will be attracted to the Cu surface as a region of low electron density. The MEP only describes the change in the electron density of an atom as a result of the addition or removal of charge [49]. As a complement to the MEP data, the Fukui function is a more accurate indicator of the part of the organic inhibitor exposed to electrophilic or nucleophilic attack.

The use of Mulliken population analysis can estimate binding sites of organic inhibitors. The calculation of the atomic charge distribution across the charge frame is widely used as a reference for determining binding sites [49]. The more negatively charged heteroatoms, the easier it is to be adsorbed on the metal surface. The local reactivity of the corrosion inhibitor can be studied by observing the Fukui index of each atom. The Fukui function provides more comprehensive information about the reactivity of the molecule being studied [49]. The Fukui function can be used to measure the local reactivity of organic inhibitors and demonstrate chemical reactivity for nucleophilic and electrophilic attacks [50-51]. Fukui function values can be used to identify which atoms in each inhibitor are more susceptible to electrophilic or nucleophilic attack. The value of the Fukui function can be calculated using Eqs. 6 and 7. The f+ value measures the reactivity side that is susceptible to nucleophilic attack associated with ELUMO to accept electrons. The f-value measures the reactivity of molecules exposed to electrophilic attack; it is related to electron-donating EHOMO [51]. Table 6 shows the nucleophilic attack (f+) of the 4HC–H inhibitor on the C9 and O19 atoms; 4HC–CH_3 nucleophilic attack occurs on the N12 and C16. Furthermore, 4HC–OCH_3 nucleophilic attack is likely to occur on the C17 and O21; while 4HC–Cl occurs in O19 and Cl21. The active site most likely accepts electrons from

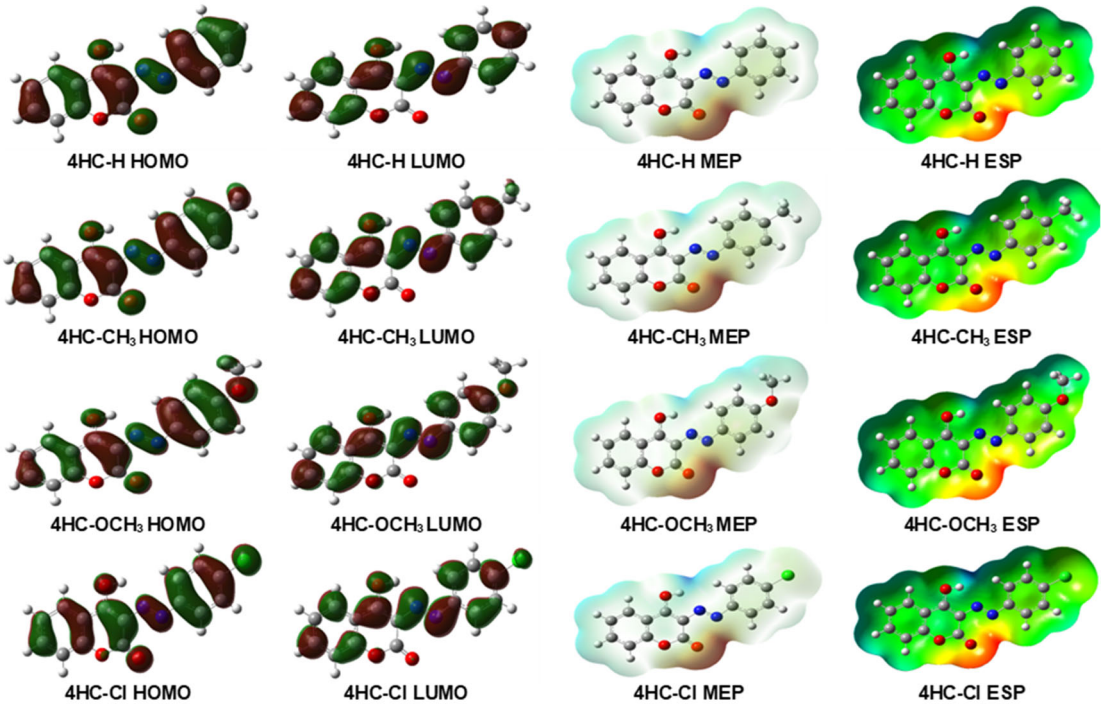

Fig 3. Visualization of the HOMO-LUMO, MEP, and ESP orbitals of 4HC-H, 4HC-CH_3, 4HC-OCH_3, 4HC-Cl

Table 6. Fukui function analysis of corrosion inhibitors 4-hydrocoumarin derivatives, 4HC-H, 4HC-CH_3, 4HC-OCH_3 and 4HC-Cl

4HC-H	N-	N	N+	f+	f-
C1	-0.4041	-0.3946	-0.3732	0.0214	0.0095
C2	-0.3776	-0.3263	-0.2889	0.0374	0.0513
C3	-0.2421	-0.2375	-0.2333	0.0041	0.0046
C4	-1.4233	-1.4690	-1.5317	-0.0626	-0.0458
C5	0.9335	0.9751	1.0491	0.0739	0.0416
C6	-0.0599	-0.0136	0.0046	0.0182	0.0463
O7	-0.1928	-0.1549	-0.1126	0.0423	0.0379
C8	0.2791	0.2855	0.2741	-0.0114	0.0063
C9	0.2159	0.2135	0.3028	**0.0893**	-0.0024
C10	0.4810	0.5575	0.6015	0.0440	0.0765
N11	-0.4339	-0.2901	-0.2231	0.0670	**0.1438**
N12	0.0525	0.2222	0.3051	0.0829	**0.1697**
C13	-0.5057	-0.6111	-0.6467	-0.0355	-0.1054
C14	0.0484	0.0928	0.1299	0.0370	0.0445
C15	-0.1607	-0.1383	-0.1107	0.0276	0.0224
C16	-0.3516	-0.3121	-0.2506	0.0615	0.0395
C17	-0.2377	-0.2026	-0.1677	0.0348	0.0352
C18	0.0568	0.1353	0.1945	0.0592	0.0784
O19	-0.3773	-0.3430	-0.2514	**0.0915**	0.0343
O20	-0.2560	-0.1876	-0.1310	0.0567	0.0684
4HC-CH_3	N-	N	N+	f+	f-
C1	-0.3980	-0.3897	-0.3728	0.0170	0.0083
C2	-0.3727	-0.3202	-0.2867	0.0336	0.0525
C3	-0.2782	-0.2756	-0.2743	0.0013	0.0026
C4	-1.3012	-1.3405	-1.3925	-0.0520	-0.0393
C5	0.9436	0.9844	1.0486	0.0642	0.0407
C6	-0.0393	0.0072	0.0240	0.0169	0.0465
C7	-0.1964	-0.1585	-0.1210	0.0374	0.0379
C8	0.2766	0.2821	0.2731	-0.0090	0.0055
C9	0.1393	0.1517	0.2249	0.0732	0.0125
C10	0.4341	0.5021	0.5451	0.0430	0.0680
N11	-0.4843	-0.3597	-0.2940	0.0657	**0.1246**
N12	0.1089	0.2951	0.3760	**0.0808**	**0.1862**
C13	-0.7795	-0.9208	-0.9724	-0.0516	-0.1413
C14	0.0636	0.1361	0.1791	0.0430	0.0725
C15	-0.6303	-0.6245	-0.6219	0.0026	0.0058
C16	0.6368	0.6776	0.7641	**0.0865**	0.0408
C17	-0.1278	-0.0740	-0.0046	0.0695	0.0537
C18	-0.0337	0.0295	0.0814	0.0520	0.0631
O19	-0.3750	-0.3405	-0.2605	0.0800	0.0345
O20	-0.2593	-0.1910	-0.1376	0.0535	0.0682
C21	-0.5677	-0.5710	-0.5747	-0.0037	-0.0034

Table 6. Fukui function analysis of corrosion inhibitors 4-hydrocoumarin derivatives, 4HC-H, 4HC-CH_3, 4HC-OCH_3 and 4HC-Cl (*Continued*)

4HC-OCH_3	N-	N	N+	f+	f-
C1	-0.3891	-0.3803	-0.3677	0.0126	0.0088
C2	-0.3957	-0.3433	-0.3169	0.0264	0.0524
C3	-0.2396	-0.2354	-0.2321	0.0034	0.0041
C4	-1.5237	-1.5689	-1.6218	-0.0529	-0.0452
C5	1.0002	1.0498	1.1044	0.0546	0.0496
C6	-0.0090	0.0362	0.0512	0.0150	0.0452
O7	-0.1953	-0.1575	-0.1268	0.0306	0.0379
C8	0.2597	0.2546	0.2466	-0.0081	-0.0051
C9	0.2366	0.2512	0.3069	0.0557	0.0146
C10	0.4550	0.5233	0.5591	0.0358	0.0683
N11	-0.4816	-0.3589	-0.2889	0.0700	**0.1227**
N12	0.0980	0.2803	0.3460	0.0657	**0.1823**
C13	-0.8710	-1.0206	-1.0535	-0.0328	-0.1496
C14	0.2856	0.3565	0.3986	0.0421	0.0709
C15	-0.3688	-0.3714	-0.3546	0.0168	-0.0026
C16	-0.3980	-0.3860	-0.3893	-0.0033	0.0120
C17	0.2840	0.3548	0.4683	**0.1135**	0.0708
C18	0.0448	0.1369	0.2140	0.0772	0.0921
O19	-0.3756	-0.3413	-0.2796	0.0617	0.0342
O20	-0.2608	-0.1933	-0.1468	0.0466	0.0674
O21	-0.2111	-0.1811	-0.0866	**0.0945**	0.0301
C22	-0.3121	-0.3236	-0.3481	-0.0245	-0.0114
4HC-Cl	N-	N	N+	f+	f-
C1	-0.3961	-0.3882	-0.3693	0.0189	0.0078
C2	-0.3625	-0.3127	-0.2768	0.0359	0.0498
C3	-0.2798	-0.2771	-0.2759	0.0012	0.0026
C4	-1.3035	-1.3419	-1.3929	-0.0511	-0.0383
C5	0.9649	1.0054	1.0770	0.0716	0.0405
C6	-0.0082	0.0360	0.0541	0.0181	0.0442
C7	-0.1901	-0.1533	-0.1137	0.0395	0.0369
C8	0.2900	0.2965	0.2860	-0.0105	0.0065
C9	0.0839	0.0865	0.1605	0.0739	0.0027
C10	0.4374	0.5026	0.5452	0.0426	0.0652
N11	-0.4995	-0.3704	-0.3100	0.0605	**0.1291**
N12	0.1302	0.3170	0.4004	0.0834	**0.1867**
C13	-0.9846	-1.1220	-1.1737	-0.0517	-0.1374
C14	0.0299	0.1105	0.1558	0.0453	0.0806
C15	-0.4149	-0.3841	-0.3499	0.0342	0.0308
C16	0.4784	0.4865	0.5036	0.0171	0.0081
C17	-0.2878	-0.2465	-0.2020	0.0445	0.0413
C18	-0.2872	-0.2289	-0.1855	0.0434	0.0583
O19	-0.3729	-0.3390	-0.2535	**0.0855**	0.0340
O20	-0.2520	-0.1847	-0.1312	0.0534	0.0673
Cl21	0.3584	0.4271	0.5569	**0.1298**	0.0687

the Cu(111) surface—the electrophilic attack (f-) of the targeted inhibitors present on atoms of N11 and N12. The active sites of N11 and N12 atoms are more likely to donate electrons to vacant orbitals to the Cu(111) surface to form coordination bonds.

Monte Carlo simulations were carried out on corrosion inhibitor systems, water molecules, and metal surfaces. Monte Carlo simulation was used to explore the adsorption properties of inhibitors and 100 molecules of H_2O on Cu(111) metal [52]. Cu(111) surface is used for the Monte Carlo simulation process because it has the most stable surface. Fig. 4 shows the most stable adsorption pattern on the Cu(111) surface containing 100 water molecules and the targeted inhibitors (4HC-H, 4HC-CH_3, 4HC-OCH_3, and 4HC-Cl). The distance between the organic corrosion inhibitor and the Cu(111) surface can determine the nature of the adsorption process [53]. In general, distances having less than 3.5 indicate that the interaction model is chemisorption, whereas lengths greater than 3.5 are associated with physisorption [53-54]. Fig. 4 shows that the distance value is less than 3.5, chemisorption's adsorption properties and a strong layer on the surface of Cu(111) can protect the copper from corrosion attack [46]. This system is also in equilibrium so that the predicted organic inhibitors are adsorbed on the Cu(111) surface. The targeted corrosion inhibitors, each having nitrogen, oxygen, and aromatic rings can donate electrons to the Cu(111) surface, respectively. The vacant orbital on the Cu(111) surface can facilitate the adsorption process by accepting electrons from the inhibitor to form a stable coordination bond [46]. Fig. 5 and Table 7 shows the adsorption energy for the most stable configuration for systems Cu(111)/4HC–H/100H_2O, Cu(111)/4HC–CH_3/100H_2O, and Cu(111)/4HC–OCH_3/100H_2O and 4HC–Cl/100H_2O. The adsorption energy of 4HC–OCH_3 is higher than that of water molecules. The distribution of adsorption energy of organic and water inhibitors can be seen in Fig. 4. It can be seen that the distribution of adsorption energy of each organic and water inhibitor is separate from each other. The 4-hydrocoumarin derivative can form a firm layer, so it is good to be used as an inhibitor of corrosion on the surface of Cu metal [52,54]. The order of adsorption energy of organic inhibitors on the surface of Cu(111) in the presence of 100 water molecules is 4HC–OCH_3 > 4HC–CH_3 > 4HC–H > 4HC–Cl. This sequence agrees with the experimental study of 4-hydrocoumarin derivatives reported by Fouda et al. [18]. The highest adsorption energy value was obtained at 137.14908 kcal/mol from

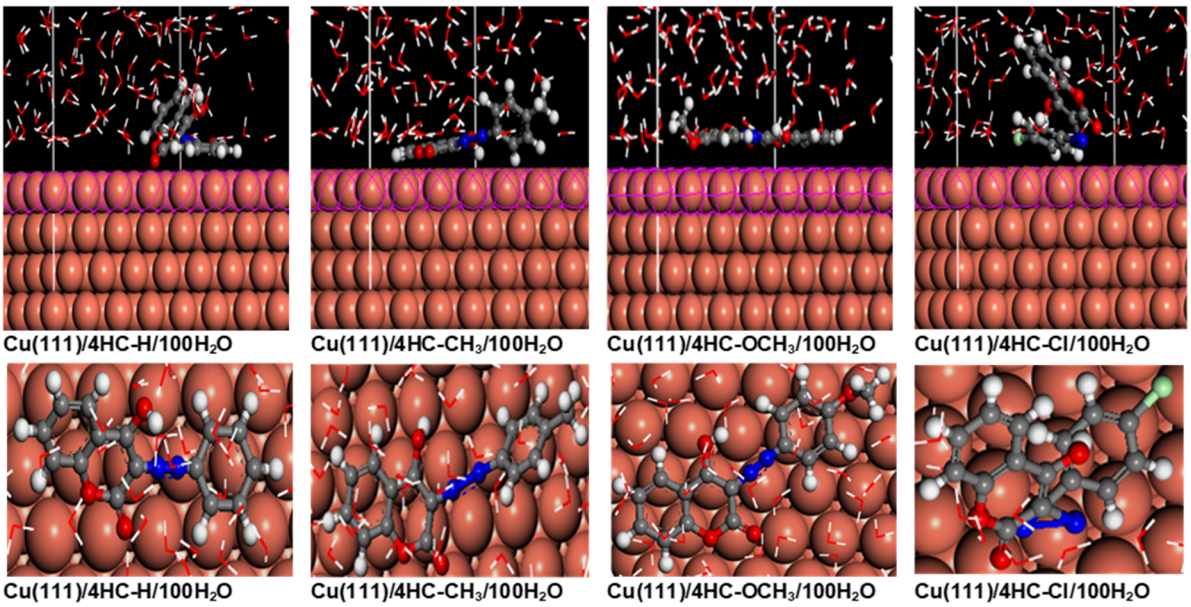

Fig 4. Adsorption of 4-hydrocoumarin derivatives on copper metal surfaces in the Monte Carlo Cu(111)/inhibitor/100H_2O system

Table 7. The adsorption energy of 4-hydrocoumarin derivative Cu(111)/inhibitor/100H_2O system calculated by Monte Carlo simulation

System	The energy of adsorption (inhibitors) kcal/mol	Adsorption energy (H_2O) kcal/mol
Inhibitor Neutral		
Cu(111)/4HC-H /100H_2O	-91.83275390	-13.39012994
Cu(111)/4HC-CH_3 /100H_2O	-103.55094600	-13.52416666
Cu(111)/4HC-OCH_3 /100H_2O	-137.14908485	-13.84864802
Cu(111)/4HC -Cl /100H_2O	-77.13014067	-16.68505331
Protonates inhibitors		
Cu(111)/4HC-H /100H_2O	-119.45137639	-14.07508940
Cu(111)/4HC-CH_3 /100H_2O	-127.25878413	-13.24084863
Cu(111)/4HC-OCH_3 /100H_2O	-133.57017060	-14.00594325
Cu(111)/4HC -Cl /100H_2O	-115.50218473	-15.79042158

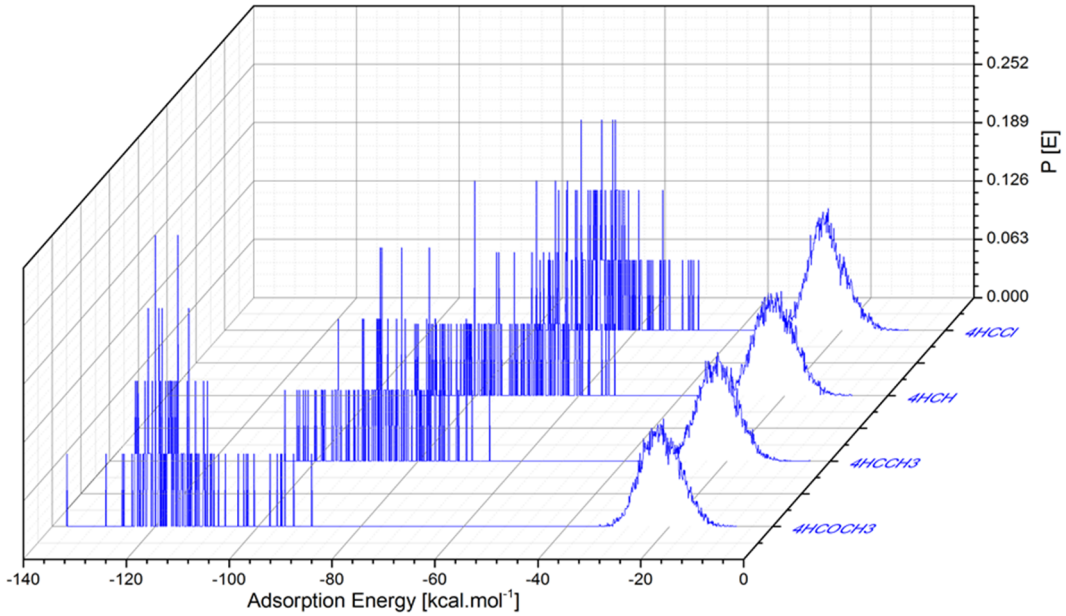

Fig 5. Distribution of the adsorption energy of the 4-hydrocoumarin derivative for the Cu(111)/inhibitor/100H_2O system

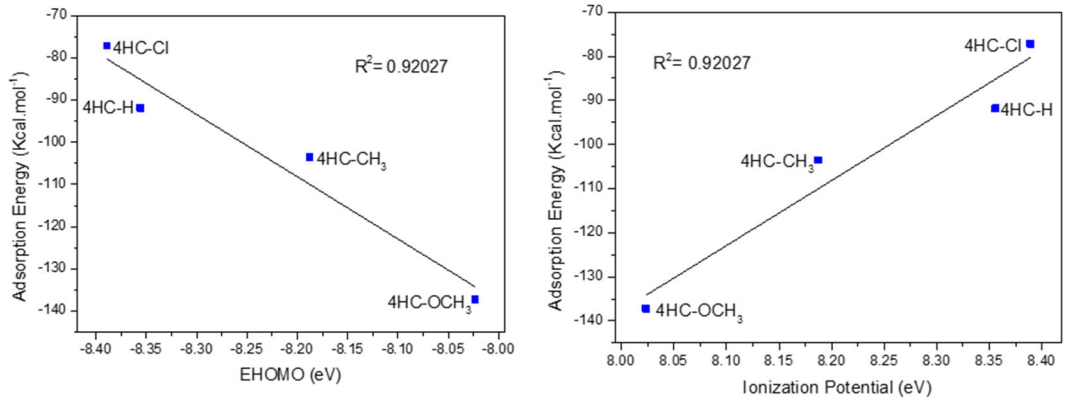

Fig 6. Correlation between adsorption energy and quantum chemical parameters of 4-hydrocoumarin derivatives from neutral conditions

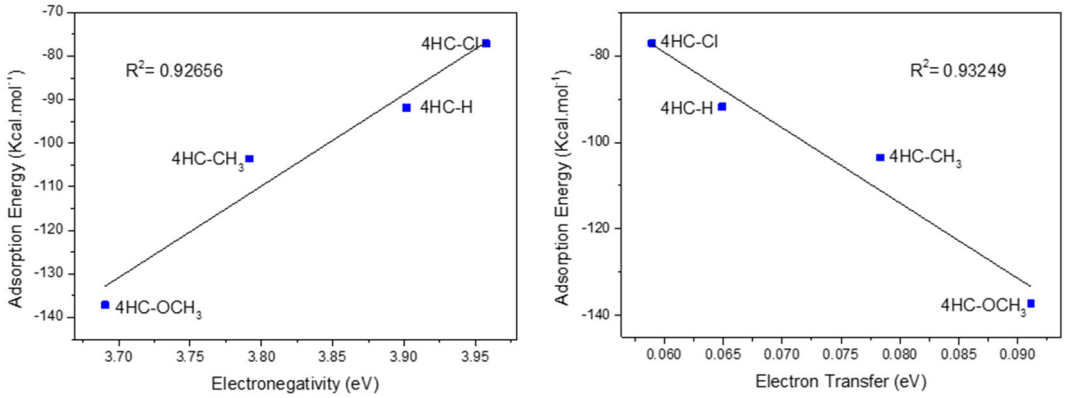

Fig 6. Correlation between adsorption energy and quantum chemical parameters of 4-hydrocoumarin derivatives from neutral conditions (*Continued*)

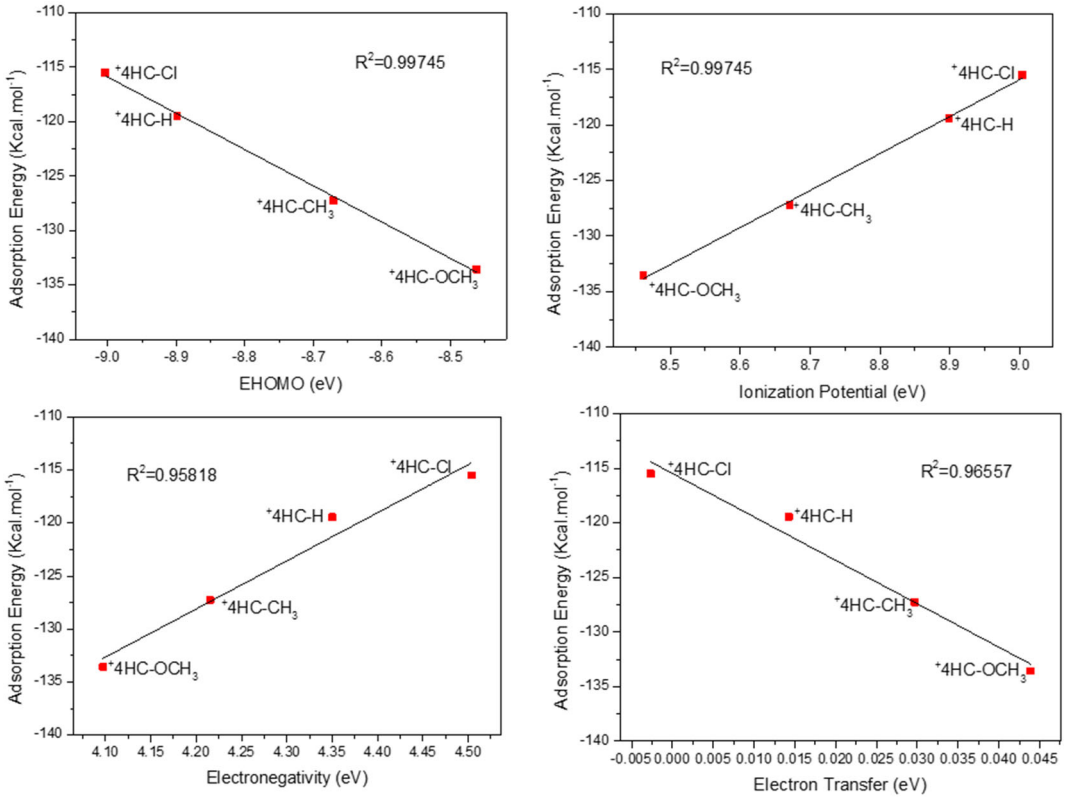

Fig 7. Correlation between adsorption energy and quantum chemical parameters of 4-hydrocoumarin derivatives under protonated inhibitor conditions

4HC–OCH_3 on the surface of Cu(111) in aqueous media. The greater the negative value of the adsorption energy, the stronger the adsorption [52-54]. That explains why 4HC–OCH_3 has high inhibitory efficiency compared to 4HC–H, 4HC–CH_3, and 4HC–Cl. The Pearson connection between adsorption energy and quantum characteristics for neutral and protonated inhibitors is shown in Fig. 6 and 7. They demonstrate linear connections, particularly for EHOMO and electron transfer. It demonstrates that these quantum factors play a significant influence in inhibitor adsorption on metal surfaces. The adsorption of inhibitor molecules on the metal surface is the general mechanism of corrosion inhibition. The adsorption energy can be used as a tool

for determining the inhibitors' amount of inhibition. The lower the inhibition energy, the more stable and stronger the adsorption of inhibitor on the metal surface.

■ CONCLUSION

Experimental studies show that 4-hydrocoumarin derivatives have potential as corrosion inhibitors. However, previous publications have not explained in detail why the 4HC–OCH_3 has the highest corrosion inhibition. Quantum chemistry calculations and Monte Carlo simulations were carried out to explain the inhibitor molecule's electronic side. Density functional theory and *ab initio* MP2 calculate quantum chemical parameters such as EHOMO, ELUMO, EGAP, ionization potential, electron affinity, electronegativity, hardness, and electron transfer on target organic inhibitors under neutral or protonated conditions. The correlation between quantum chemical parameters such as EHOMO, ionization potential, electronegativity, electron transfer with adsorption energy provides an excellent correlation. Quantum parameters explain why OCH_3 functional group has the highest corrosion inhibition while the chlorine group gives the lowest yield. In addition, the highest adsorption energy of 4HC–OCH_3 also supports the previous explanation. The highest adsorption energy was obtained at 4HC–OCH_3, with a value of -137.1490 kcal/mol, followed by 4HC–CH_3 > 4HC–H > 4HC–Cl. The study is expected to strengthen the explanation of the experimental study.

■ REFERENCES

[1] Chaubey, N., Savita, S., Qurashi, A., Chauhan, D.S., and Quraishi, M.A., 2020, Frontiers and advances in green and sustainable inhibitors for corrosion applications: A critical review, *J. Mol. Liq.*, 321, 114385.

[2] Hossain, N., Chowdhury, M.A., and Kchaou, M., 2021, An overview of green corrosion inhibitors for sustainable and environment friendly industrial development, *J. Adhes. Sci. Technol.*, 35 (7), 673–690.

[3] Chauhan, D.S., Quraishi, M.A., and Qurashi, A., 2021, Recent trends in environmentally sustainable sweet corrosion inhibitors, *J. Mol. Liq.*, 326, 115117.

[4] Verma, C., Ebenso, E.E., Quraishi, M.A., and Hussain, C.M., 2021, Recent developments in sustainable corrosion inhibitors: Design, performance and industrial scale applications, *Mater. Adv.*, 2 (2), 3806–3850.

[5] Verma, C., Haque, J., Quraishi, M.A., and Ebenso, E.E., 2019, Aqueous phase environmental friendly organic corrosion inhibitors derived from one step multicomponent reactions: A review, *J. Mol. Liq.*, 275, 18–40.

[6] Montemor, M.F., 2016, "Fostering green inhibitors for corrosion prevention" in *Active Protective Coatings*, *Springer Series in Materials Science, vol 233*, Eds. Hughes, A., Mol, J., Zheludkevich, M., and Buchheit, R., Springer, Dordrecht, 107–137.

[7] Umoren, S.A., Solomon, M.M., Madhankumar, A., and Obot, I.B., 2020, Exploration of natural polymers for use as green corrosion inhibitors for AZ31 magnesium alloy in saline environment, *Carbohydr. Polym.*, 230, 115466.

[8] Dutta, A., Saha, S.K., Adhikari, U., Banerjee, P., and Sukul, D., 2017, Effect of substitution on corrosion inhibition properties of 2-(substituted phenyl) benzimidazole derivatives on mild steel in 1 M HCl solution: A combined experimental and theoretical approach, *Corros. Sci.*, 123, 256–266.

[9] Berisha, A., 2022, An experimental and theoretical investigation of the efficacy of pantoprazole as a corrosion inhibitor for mild steel in an acidic medium, *Electrochem*, 3 (1), 28–41.

[10] Upadhyay, A., Purohit, A.K., Mahakur, G., Dash, S., and Kar, P.K., 2021, Verification of corrosion inhibition of mild steel by some 4-aminoantipyrine-based Schiff bases – Impact of adsorbate substituent and cross-conjugation, *J. Mol. Liq.*, 333, 115960.

[11] Hadisaputra, S., Purwoko, A.A., Ilhamsyah, I., Hamdiani, S., Suhendra, D., Nuryono, N., and Bundjali, B., 2018, A combined experimental and theoretical study of (E)-ethyl 3-(4-methoxyphenyl) acrylate as corrosion inhibitor of iron in 1 M HCl solutions, *Int. J. Corros. Scale Inhib.*, 7 (4), 633–647.

[12] Xu, S., Zhang, S., Guo, L., Feng, L., and Tan, B., 2019, Experimental and theoretical studies on the corrosion inhibition of carbon steel by two indazole derivatives in HCl medium, *Materials*, 12 (8), 1339.

[13] Zhao, W., Chang, T., Leygraf, C., and Johnson, C.M., 2021, Corrosion inhibition of copper with octadecylphosphonic acid (ODPA) in a simulated indoor atmospheric environment, *Corros. Sci.*, 192, 109777.

[14] Tan, B., Zhang, S., Qiang, Y., Li, W., Liu, H., Xu, C., and Chen, S., 2019, Insight into the corrosion inhibition of copper in sulfuric acid via two environmentally friendly food spices: Combining experimental and theoretical methods, *J. Mol. Liq.*, 286, 110891.

[15] Dahmani, K., Galai, M., Ouakki, M., Cherkaoui, M., Touir, R., Erkan, S., Kaya, S., and El Ibrahimi, B., 2021, Quantum chemical and molecular dynamic simulation studies for the identification of the extracted cinnamon essential oil constituent responsible for copper corrosion inhibition in acidified 3.0 wt% NaCl medium, *Inorg. Chem. Commun.*, 124, 108409.

[16] Refait, P., Rahal, C., and Masmoudi, M., 2020, Corrosion inhibition of copper in 0.5 M NaCl solutions by aqueous and hydrolysis acid extracts of olive leaf, *J. Electroanal. Chem.*, 859, 113834.

[17] Jmiai, A., Tara, A., El Issami, S., Hilali, M., Jbara, O., and Bazzi, L., 2021, A new trend in corrosion protection of copper in acidic medium by using Jujube shell extract as an effective green and environmentally safe corrosion inhibitor: Experimental, quantum chemistry approach and Monte Carlo simulation study, *J. Mol. Liq.*, 322, 114509.

[18] Fouda, A.S., Rashwan, S.M., Kamel, M.M., and Khalifa, M.M., 2016, 4-Hydroxycoumarin derivatives as corrosion inhibitors for copper in nitric acid solutions, *J. Mater. Environ. Sci.*, 7 (8), 2658–2678.

[19] Hajiahmadi, Z., and Tavangar, Z., 2019, Extensive theoretical study of corrosion inhibition efficiency of some pyrimidine derivatives on iron and the proposal of new inhibitor, *J. Mol. Liq.*, 284, 225–231.

[20] Assad, H., and Kumar, A., 2021, Understanding functional group effect on corrosion inhibition efficiency of selected organic compounds, *J. Mol. Liq.*, 344, 117755.

[21] Kumar, D., Jain, N., Jain, V., and Rai, B., 2020, Amino acids as copper corrosion inhibitors: A density functional theory approach, *Appl. Surf. Sci.*, 514, 145905.

[22] Chiter, F., Costa, D., Maurice, V., and Marcus, P., 2021, DFT investigation of 2-mercaptobenzothiazole adsorption on model oxidized copper surfaces and relationship with corrosion inhibition, *Appl. Surf. Sci.*, 537, 147802.

[23] Hadisaputra, S., Purwoko, A.A., Wajdi, F., Sumarlan, I., and Hamdiani, S., 2019, Theoretical study of the substituent effect on corrosion inhibition performance of benzimidazole and its derivatives, *Int. J. Corros. Scale Inhib.*, 8 (3), 673–688.

[24] Behzadi, H., Roonasi, P., Momeni, M.J., Manzetti, S., Esrafili, M.D., Obot, I.B., Yousefvand, M., and Mousavi-Khoshdel, S.M., 2015, A DFT study of pyrazine derivatives and their Fe complexes in corrosion inhibition process, *J. Mol. Struct.*, 1086, 64–72.

[25] Garcia-Ochoa, E., Guzmán-Jiménez, S.J., Hernández, J.G., Pandiyan, T., Vásquez-Pérez, J.M., and Cruz-Borbolla, J., 2016, Benzimidazole ligands in the corrosion inhibition for carbon steel in acid medium: DFT study of its interaction on Fe_{30} surface, *J. Mol. Struct.*, 1119, 314–324.

[26] Costa, D., Ribeiro, T., Cornette, P., and Marcus, P., 2016, DFT modeling of corrosion inhibition by organic molecules: Carboxylates as inhibitors of aluminum corrosion, *J. Phys. Chem. C*, 120 (50), 28607–28616.

[27] Dao, D.Q., Hieu, T.D., Pham, T.L.M., Tuan, D., Nam, P.C., and Obot, I.B., 2017, DFT study of the interactions between thiophene-based corrosion

inhibitors and an Fe_4 cluster, *J. Mol. Model.*, 23 (9), 260.

[28] Obot, I.B., Macdonald, D.D., and Gasem, Z.M., 2015, Density functional theory (DFT) as a powerful tool for designing new organic corrosion inhibitors. Part 1: An overview, *Corros. Sci.*, 99, 1–30.

[29] Sengupta, S., Murmu, M., Murmu, N.C., and Banerjee, P., 2021, Adsorption of redox-active Schiff bases and corrosion inhibiting property for mild steel in 1 mol L^{-1} H_2SO_4: Experimental analysis supported by *ab initio* DFT, DFTB and molecular dynamics simulation approach, *J. Mol. Liq.*, 326, 115215.

[30] Obot, I.B., Haruna, K., and Saleh, T.A., 2019, Atomistic simulation: A unique and powerful computational tool for corrosion inhibition research, *Arabian J. Sci. Eng.*, 44 (1), 1–32.

[31] Zhu, Y., Sun, Q., Wang, Y., Tang, J., and Wang, Y., 2020, A study on inhibition performance of mercaptoalcohols as corrosion inhibitors by first principle and molecular dynamics simulation, *Russ. J. Phys. Chem. A*, 94 (9), 1877–1886.

[32] Kasprzhitskii, A., and Lazorenko, G., 2021, Corrosion inhibition properties of small peptides: DFT and Monte Carlo simulation studies, *J. Mol. Liq.*, 331, 115782.

[33] Shamov, G.A., Schreckenbach, G., Martin, R.L., and Hay, P.J., 2008, Crown ether inclusion complexes of the early actinide elements, $[AnO_2(18\text{-crown-}6)]^{n+}$, An = U, Np, Pu and n= 1, 2: A relativistic density functional study, *Inorg. Chem.*, 47 (5), 1465–1475.

[34] Pan, Q.J., and Schreckenbach, G., 2010, Binuclear hexa-and pentavalent uranium complexes with a polypyrrolic ligand: A density functional study of water-and hydronium-induced reactions, *Inorg. Chem.*, 49 (14), 6509–6517.

[35] Fan, Y., Li, Y., Shu, X., Wu, R., Chen, S., Jin, Y., Xu, C., Chen, J., Huang, C., and Xia, C., 2021, Complexation and separation of trivalent actinides and lanthanides by a novel DGA derived from macrocyclic crown ether: Synthesis, extraction, and spectroscopic and density functional theory studies, *ACS Omega*, 6 (3), 2156–2166.

[36] Frisch, M.J., Trucks, G.W., Schlegel, H.B., Scuseria, G.E., Robb, M.A., Cheeseman, J.R., Scalmani, G., Barone, V., Petersson, G.A., Nakatsuji, H., Li, X., Caricato, M., Marenich, A., Bloino, J., Janesko, B.G., Gomperts, R., Mennucci, B., Hratchian, H.P., Ortiz, J.V., Izmaylov, A.F., Sonnenberg, J.L., Williams-Young, D., Ding, F., Lipparini, F., Egidi, F., Goings, J., Peng, B., Petrone, A., Henderson, T., Ranasinghe, D., Zakrzewski, V.G., Gao, J., Rega, N., Zheng, G., Liang, W., Hada, M., Ehara, M., Toyota, K., Fukuda, R., Hasegawa, J., Ishida, M., Nakajima, T., Honda, Y., Kitao, O., Nakai, H., Vreven, T., Throssell, K., Montgomery, Jr., J.A., Peralta, J.E., Ogliaro, F., Bearpark, M., Heyd, J.J., Brothers, E., Kudin, K.N., Staroverov, V.N., Keith, T., Kobayashi, R., Normand, J., Raghavachari, K., Rendell, A., Burant, J.C., Iyengar, S.S., Tomasi, J., Cossi, M., Millam, J.M., Klene, M., Adamo, C., Cammi, R., Ochterski, J.W., Martin, R.L., Morokuma, K., Farkas, O., Foresman, J.B., and Fox, D.J., 2016, *Gaussian 09, Revision A.02*, Gaussian, Inc., Wallingford CT.

[37] Islam, N., and Ghosh D.C., 2011, A new algorithm for the evaluation of the global hardness of polyatomic molecules, *Mol. Phys.*, 109 (6), 917–931.

[38] Parr, R.G., Szentpaly, L.V., and Liu, S., 1999, Electrophilicity index, *J. Am. Chem. Soc.*, 121 (9), 1922–1924.

[39] Yang, W., and Parr, R.G., 1985, Hardness, softness, and the Fukui function in the electronic theory of metals and catalysis, *Proc. Natl. Acad. Sci. U. S. A.*, 82 (20), 6723–6726.

[40] Pearson, R.G., 1990, Hard and soft acids and bases—The evolution of a chemical concept, *Coord. Chem. Rev.*, 100, 403–425.

[41] Pearson, R.G., 1988, Absolute electronegativity and hardness: Application to inorganic chemistry, *Inorg. Chem.*, 27 (4), 734–740.

[42] Sastri, V.S., and Perumareddi, J.R., 1997, Molecular orbital theoretical studies of some organic corrosion inhibitors, *Corrosion*, 53 (8), 617–622.

[43] Guo, L., Safi, Z.S., Kaya, S., Shi, W., Tüzün, B., Altunay, N., and Kaya, C., 2018, Anticorrosive

effects of some thiophene derivatives against the corrosion of iron: A computational study, *Front. Chem.*, 6, 00155.

[44] Frenkel, D., and Smit, B., 2002, *Understanding Molecular Simulations: From Algorithms to Applications*, 2nd Ed., Academic Press, San Diego.

[45] Kirkpatrick, S., Gelatt, C.D., and Vecchi, M.P., 1983, Optimization by simulated annealing, *Science*, 220 (4598), 671–680.

[46] Hadisaputra, S., Purwoko, A.A., Savalas, L.R.T., Prasetyo, N., Yuanita, E., and Hamdiani, S., 2020, Quantum chemical and Monte Carlo simulation studies on inhibition performance of caffeine and its derivatives against corrosion of copper, *Coatings*, 10 (11), 1086.

[47] Stefanou, V., Matiadis, D., Melagraki, G., Afantitis, A., Athanasellis, G., Igglessi-Markopoulou, O., McKee, V., and Markopoulos, J., 2011, Functionalized 4-hydroxy coumarins: Novel synthesis, crystal structure and DFT calculations, *Molecules*, 16 (1), 384–402.

[48] Sagdinc, S., Kara, Y., and Kayadibi, F., 2014, Theoretical study of 11-thiocyanatoundecanoic acid phenylamide derivatives on corrosion inhibition efficiencies, *Can. J. Chem.*, 92 (9), 876–887.

[49] Şahin, M., Gece, G., Karcı, F., and Bilgiç, S., 2008, Experimental and theoretical study of the effect of some heterocyclic compounds on the corrosion of low carbon steel in 3.5% NaCl medium, *J. Appl. Electrochem.*, 38 (6), 809–815.

[50] Saranya, J., Sounthari, P., Parameswari, K., and Chitra, S., 2016, Acenaphtho[1,2-b]quinoxaline and acenaphtho[1,2-b]pyrazine as corrosion inhibitors for mild steel in acid medium, *Measurement*, 77, 175–186.

[51] Saha, S.K., Ghosh, P., Hens, A., Murmu, N.C., and Banerjee, P., 2015, Density functional theory and molecular dynamics simulation study on corrosion inhibition performance of mild steel by mercapto-quinoline Schiff base corrosion inhibitor, *Phys. E*, 66, 332–341.

[52] Tan, J., Guo, L., Wu, D., Wang, S., Yu, R., Zhang, F., and Kaya, S., 2020, Electrochemical and computational studies on the corrosion inhibition of mild steel by 1-hexadecyl-3-methylimidazolium bromide in HCl medium, *Int. J. Electrochem. Sci.*, 15, 1893–1903.

[53] Huong, D.Q., Lan Huong, N.T., Anh Nguyet, T.T., Duong, T., Tuan, D., Thong, N.M., and Nam, P.C., 2020, Pivotal role of heteroatoms in improving the corrosion inhibition ability of thiourea derivatives, *ACS Omega*, 5 (42), 27655–27666.

[54] Chauhan, D.S., Verma, C., and Quraishi, M.A., 2021, Molecular structural aspects of organic corrosion inhibitors: Experimental and computational insights, *J. Mol. Struct.*, 1227, 129374.